Research on Evaluation Method of Rockburst Proneness Based on Energy Principles

Feiyue Sun
Henan Polytechnic University
Wenlong Wu (hpuwwl@qq.com)
Henan Polytechnic University

Research Article

Keywords: Energy principle, Rockburst proneness criterion, Rockburst classification thresholds, Rockburst disaster, Numerical simulation analysis

Posted Date: April 21st, 2021

DOI: https://doi.org/10.21203/rs.3.rs-437275/v1

Research on evaluation method of rockburst proneness based on energy principles

Feiyue Sun[1, 2], Wenlong Wu[1, 2 *]

1 School of Civil Engineering, Henan Polytechnic University, Jiaozuo 454000, Henan, China

2 Key Laboratory of Henan Province for Underground Engineering and Disaster Prevention, Jiaozuo 454000, Henan, China

*Correspondence e-mail: hpuwwl@qq.com

Abstract: The study of rockburst criterion is the key to predict whether rockburst occurs or not. First of all, based on the energy principle and taking the rock strength and overall failure criterion as the benchmark, the rockburst proneness criterion of rock mass unit under compression and tension was established. The criterion took into account the integrity factors, mechanical factors, brittleness factors and energy storage factors in the process of rockburst inoculation, and three rockburst classification thresholds (2, 11 and 110) for four grades of none, weak, moderate and severe rockburst were proposed. Second, Taking the typical rockburst disaster as examples, the rationality of the existing classical rockburst criterions and the rockburst proneness criterion proposed in this paper were tested, and the results showed that this criterion had good engineering applicability. Finally, the numerical simulation analysis of rockburst disaster in $2^{\#}$ diversion tunnel of Jinping II hydropower station was carried out by using this criterion. The results were basically consistent with the actual situation, which verified the accuracy and effectiveness of the rockburst proneness criterion proposed in this paper. The research results can provide reference for the

evaluation and prediction of rockburst disaster in deep underground engineering.

Keywords: Energy principle; Rockburst proneness criterion; Rockburst classification thresholds; Rockburst disaster; Numerical simulation analysis

1 Introduction

Since the first rockburst occurred in the South Stafford tin mine in the United Kingdom in 1738, many countries and regions have experienced rockburst disasters worldwide, such as South Africa, India, Japan, the United States, France, Switzerland, etc. (Feng et al. 2012, Ma et al. 2015, Wei et al. 2020) The earliest recorded coal-burst in China occurred in the Shengli Coal Mine of Fushun in 1933 (Zhang and Fu, 2008). After that, rockburst frequently occurred in traffic tunnels, hydraulic tunnels and other underground cavern projects in China. Rockburst is a dynamic instability phenomenon of sudden burst caused by the instantaneous release of elastic deformation energy accumulated in rock mass in the process of underground engineering excavation, which is often accompanied by rock ejection or throwing, strong vibration, huge sound and air waves, etc. (Feng et al. 2019) Rockburst has strong suddenness, locality, concealment and harmfulness, which greatly threatens the safety of on-site construction personnel and mechanical equipment, and brings serious challenges to the design and construction of deep engineering (Roohollah and Abbas, 2018). Therefore, with the vigorous development of deep underground engineering construction in the world, it is urgent to continuously study the mechanism of rockburst, accurately grasp the law of rockburst inoculation and evolution and the possibility of rockburst occurrence, and accurately predict the strength of rockburst activities. This is of great theoretical significance and engineering application value to ensure the safety and healthy development of underground engineering

45 construction.

46 At present, rock mechanics workers and engineering technicians at home and abroad have
47 carried out in-depth research on rockburst criterion and rockburst classification from theoretical
48 analysis, numerical simulation, field monitoring and test under the guidance of deep rock mass
49 mechanics and nonlinear dynamic science theory, and put forward corresponding prediction and
50 evaluation indexes based on their respective assumptions. In the study of rockburst criterion and
51 rockburst classification theory, many experts and scholars have proposed dozens of classical
52 rockburst criteria and intensity classification successively, such as E. Hoek criterion, Russnes
53 criterion, Turchaninov criterion, Kidybinski energy criterion, Motycaka energy ratio method, Barton
54 criterion, Erlangshan highway tunnel criterion and Gu-Tao criterion, etc. (Hoek and Brown 1997;
55 Russnes 1974; John and Neville 1974; Kidybinnski 1981; Zhang et al. 2017; Barton et al. 1974; Xu
56 and Wang 1999; Gu et al. 2002) In the field monitoring research, scholars have achieved some
57 fruitful research results, such as microseismic monitoring method, acoustic emission monitoring
58 method, microgravity method, acoustic wave detection method, infrared thermal imaging method
59 and so on (Wu 1993; Chen et al. 2010; Zhang et al. 2012; Zhang et al. 2018; Zhang et al. 2020). In
60 the aspect of experimental study on rockburst criterion, some experts at home and abroad have also
61 carried out some research. Karchevsky (2017) proposed a calculating quantity algorithm through
62 experimental research, and took this algorithm as a standard to distinguish the possibility of rock
63 fracture in coal seam. Li et al. (2018) proposed failure criterion of rock strength based on energy
64 mutation. Li et al. (2019) put forward a rockburst dynamic criterion based on dynamic and static
65 energy index. Gong et al. (2020) advanced a rockburst proneness classification standard based on
66 the failure results and phenomena of rock samples tested in laboratory tests. With the rapid

development of computer technology, numerical analysis method emerges as the times require and becomes more and more perfect. Based on energy theory, scholars have propounded different numerical indexes of rockburst criteria, such as Energy release rate (ERR), Excess shear stress (ESS), Burst potential index (BPI), Local energy release density (LERD), Local energy release rate (LERR), Relative energy release index (RERI), Unit time relative local energy release index (URLERI), etc. (Cook 1965; Ryder 1988; Mitri 1999; WILES 1998; Su 2006; Qiu et al. 2014; BIENIAWSKI 1967)

The above achievements greatly promote the development of the rockburst criterion research. However, due to the complex conditions and many influencing factors of rock burst, the existing rock burst criterions only consider one or two of the influencing factors, resulting in its theoretical research far behind the engineering practice, and there are still deficiencies in engineering applicability. In view of this, this study attempts to establish a rockburst proneness criterion and based on energy principle on the basis of fully collecting, summarizing and deeply analyzing the existing rockburst criterions at home and abroad, so as to provide basic scientific basis and important theoretical support for rockburst prediction.

2 Energy conversion mechanism of deformation process of rock under stress

The deformation and failure of rock is mainly driven by energy. From the energy point of view, when the rock is deformed under the action of external force, assuming that the physical process has no heat exchange with the outside world, the total input energy generated by the external force is U. According to the principle of energy conservation, the expression of U can be obtained (Xie et al. 2005):

$$U = U^{d} + U^{e} \tag{1}$$

Where U^{d} is the dissipated energy of the rock, which is used to form the internal damage and plastic deformation of the material, as shown in the blank area surrounded by the curve in **Fig. 1**; U^{e} is the releasable elastic strain energy of the rock, as shown in the shadow area surrounded by the curve in **Fig. 1**.

Fig. 1 Stress-strain relation curve of rock

The expression of U^{e} is

$$U^{e} = \left[\sigma_1^2 + \sigma_2^2 + \sigma_3^2 - 2\nu\left(\sigma_1\sigma_2 + \sigma_2\sigma_3 + \sigma_1\sigma_3\right)\right]/2E \tag{2}$$

Where $\sigma_1, \sigma_2, \sigma_3$ is the three principal stresses corresponding to the maximum value of element strain energy; E is the elastic modulus; and ν is the Poisson's ratio.

Based on the energy transformation in the process of rock deformation, the difference between dynamic and static failure of rock is explained. The rock is disturbed by the dynamic load to form high stress, which leads to the aggravation of damage of some rock units in a very short period of time and the gradual decrease of strength; the stored elastic strain energy of most rocks rapidly reaches the limit value. U^{0} represents the energy required when the rock mass is broken. When $U^{e} = U^{0}$, U^{e} completely releases and rock mass undergoes static failure; When $U^{e} > U^{0}$, the rock mass is damaged dynamically, and the energy difference ΔU ($\Delta U = U^{e} - U^{0}$) constitutes the kinetic energy of splitting rock mass, which induces rockburst.

3 Rockburst proneness criterion based on energy principle

3.1 Shortcomings of existing rockburst criterions

The existing rockburst accident cases show that rockburst mostly occurs in brittle rock mass

111 under the conditions of lithologically medium-hard to hard, good integrity, dry and high geostress.
112 At present, the rockburst criterion for underground engineering mainly considers the following
113 indicators: maximum principal stress of cavern (σ_1), maximum tangential stress of cavern (σ_θ), radial
114 stress of cavern (σ_r), uniaxial compressive strength of rock (σ_c), tensile strength of rock (σ_t), elastic
115 energy index of rock (W_{et}), integrity coefficient of rock mass (K_v)and lateral pressure coefficient (λ),
116 etc.

117 Through in-depth analysis of existing rockburst criterions, it is known that (1) Most rockburst
118 criteria are expressed by radial stress and tangential stress (or maximum tangential stress).
119 Coordinate transformation is needed when using numerical simulation software to predict and
120 evaluate rockburst risk in underground engineering excavation process, so the application is quite
121 complicated (Xu et al. 2007; Guo et al. 2015). (2) The evaluation index of rockburst criterion is
122 single, only one or two factors are considered, and the influencing factors of rockburst are not fully
123 considered. (3) According to the definition of rockburst, the surrounding rock stress is one of the
124 necessary conditions to induce rock burst (Wang et al. 1998), and the surrounding rock in the
125 rockburst area is mostly in the three-dimensional stress state, but the existing rockburst criteria are
126 mostly expressed by the maximum principal stress or the maximum tangential stress and the two-
127 dimensional stress state. (4) Most rock burst classifications are more general and the discriminant
128 indexes used are also different.

129 **3.2 Establishment of rockburst proneness criterion**

130 To establish rockburst criterion based on energy principle, it is necessary to clarify the energy
131 evolution law in the process of rock deformation and failure. In this study, based on the rock strength
132 and overall failure criterion (Xie et al. 2005), the rockburst criteria and rockburst classification

133 standards for rock mass units under compression and tension are given respectively.

134 **3.2.1 Compression condition ($\sigma_1 > \sigma_2 > \sigma_3 \geqslant 0$)**

135 A large number of underground engineering practice shows that the stress state of surrounding
136 rock before underground cavern excavation is mostly three-dimensional compression (**Fig. 2(a)**).
137 When the rock mass fails as a whole, the elastic strain energy in the principal stress σ_i direction is
138 proportional to the energy release rate, which is distributed according to the minimum compressive
139 stress difference. Assuming that the energy release rate G_i is expressed as:

140 $$G_i = K_i \left(\sigma_1 - \sigma_i\right) U^{\mathrm{e}} \quad (i = 1,\ 2,\ 3) \tag{3}$$

141 Where K_i is the material constant.

142 (a) Compression condition (b) Tension condition

143 **Fig. 2** Loading condition

144 It can be seen from **Eq.** (3) that the maximum energy release rate occurs in the direction of the
145 minimum compressive stress σ_3, i.e

146 $$G_3 = K_i \left(\sigma_1 - \sigma_3\right) U^{\mathrm{e}} \tag{4}$$

147 This further shows that the hydrostatic pressure state will not cause the overall failure of rock
148 mass. According to the above analysis, the energy release rate can meet the following requirements
149 when rockburst occurs:

150 $$G_i = K_i \left(\sigma_1 - \sigma_i\right) U^{\mathrm{e}} \geq G_{\mathrm{c}} \tag{5}$$

151 Where G_{c} is the critical strain energy release rate of rockburst under compression state, which is the
152 material constant and can be determined by laboratory rock mechanics test (uniaxial compression
153 test). Let $\sigma_1=\sigma_{\mathrm{c}}$ and $\sigma_2=\sigma_3=0$, bring them into **Eq.** (5), it can be obtained by combining **Eq.** (2):

154 $$G_{\mathrm{c}} = K_{\mathrm{i}} \frac{\sigma_{\mathrm{c}}^3}{2E} \tag{6}$$

Further considering the influence of rock mass integrity coefficient (K_v) on inducing rockburst, combining **Eqs.** (3)–(6), a rockburst proneness criterion (RPC_c) based on the energy principle (triaxial compression state of rock mass) is established:

$$RPC_c = K_v^2 \cdot \frac{G_3}{G_c} = K_v^2 \cdot \frac{(\sigma_1 - \sigma_3) 2EU^e}{\sigma_c^3} = K_v^2 \cdot \frac{\sigma_1 - \sigma_3}{\sigma_c} \cdot \frac{\sigma_c \sigma_t}{\sigma_t} \cdot \frac{2EU^e}{\sigma_c^3} = K_v^2 \cdot (\sigma_1 - \sigma_3) \sigma_t \cdot \frac{\sigma_c}{\sigma_t} \cdot \frac{2EU^e}{\sigma_c^4} \quad (7)$$

It can be seen from **Eq.** (7) that: (1) RPC_c analysis model reflects the integrity factor (K_v), mechanical factor ($(\sigma_1-\sigma_3)\sigma_t$), brittleness factor ($\sigma_c/\sigma_t$) and energy storage factor (U^e/σ_c^4) of rockburst incubation process; (2) RPC_c is the product of main stress in mathematical expression, which is easy to understand, use and operate; (3) RPC_c not only considers the stress state (σ_1, σ_2, σ_3) of surrounding rock and the integrity of rock mass, but also reflects the influence of rock mechanical parameters (σ_c, σ_t) and deformation parameters (E, v).

3.2.2 Tension condition ($\sigma_3 < 0$)

Tensile stress often occurs in the surrounding rock mass during excavation and unloading of underground engineering, which is also a stress state leading to the overall failure of rock mass. When there is at least one tensile stress in the principal stress (σ_i) of rock element (**Fig. 2(b)**) and the overall failure of rock mass occurs, the elastic strain energy is proportional to the energy release rate in the direction of principal stress, and it is distributed according to the principal stress value. Assuming that the energy release rate expression is:

$$G_i = K_i \sigma_i U^e \quad (i = 1,\ 2,\ 3) \quad (8)$$

By analogy with compression condition, it can be seen from **Eq.** (8) that the maximum energy release rate occurs in the direction of the maximum tensile stress σ_3, i.e

$$G_3 = K_i \sigma_3 U^e \quad (9)$$

The energy release rate can meet the following requirements when rockburst occurs:

$$G_i = K_i \sigma_i U^{\mathrm{e}} \geq G_{\mathrm{t}} \tag{10}$$

Where G_{t} is the critical strain energy release rate of rockburst under tension state, which is the material constant and can be determined by laboratory rock mechanics test (uniaxial tensile test). Let $\sigma_3=\sigma_{\mathrm{t}}$ and $\sigma_1=\sigma_2=0$, bring them into **Eq.** (10), it can be obtained by combining **Eq.** (2):

$$G_{\mathrm{t}} = K_i \frac{\sigma_{\mathrm{t}}^3}{2E} \tag{11}$$

Further considering the influence of rock mass integrity coefficient (K_{v}) on inducing rockburst, combining **Eqs.** (8)–(11), a rockburst proneness criterion ($\mathrm{RPC_t}$) based on the energy principle (tension state of rock mass) is established:

$$\mathrm{RPC_t} = K_{\mathrm{v}}^2 \cdot \frac{G_3}{G_{\mathrm{t}}} = K_{\mathrm{v}}^2 \cdot \frac{2EU^{\mathrm{e}}\sigma_3}{\sigma_{\mathrm{t}}^3} = K_{\mathrm{v}}^2 \cdot \frac{\sigma_3}{\sigma_{\mathrm{c}}} \cdot \frac{\sigma_{\mathrm{c}}}{\sigma_{\mathrm{t}}} \cdot \frac{2EU^{\mathrm{e}}}{\sigma_{\mathrm{t}}^2} \tag{12}$$

By analogy with compression condition, it can be seen from **Eq.** (12) that when rock mass is in tensile state, $\mathrm{RPC_t}$ also reflects the integrity factor (K_{v}), mechanical factor ($\sigma_3/\sigma_{\mathrm{c}}$), brittleness factor ($\sigma_{\mathrm{c}}/\sigma_{\mathrm{t}}$) and energy storage factor ($U^{\mathrm{e}}/\sigma_{\mathrm{t}}^2$) of rockburst incubation process.

In order to determine the threshold value of the rockburst proneness criterion, based on the division of the elastic energy index threshold value and the rockburst potential threshold value (Zhang et al. 2011; Shang et al. 2013), the measured rockburst data of Tiantaishan tunnel (**Table 1**) (Guo et al. 2015) are taken as simulation samples for analysis, and the results are shown in **Table 2** (Guo et al. 2015; Ministry of Water Resources of the People's Republic of China 2014).

Table 1 Measured data of rockburst of Tiantaishan tunnel

Table 2 Simulation results of rockburst of Tiantaishan tunnel

Considering that the probability of the boundary index of different factors reaching the maximum value at the same time is small, in order to facilitate practical application, the boundary indexes of RPC are set to 2, 11 and 110. Therefore, the rockburst proneness criterion and its intensity

199 classification are as follows:

200
$$\mathrm{RPC}=\begin{cases}<2 & \text{None rockburst}\\ 2-11 & \text{Weak rockburst}\\ 11-110 & \text{Moderate rockburst}\\ >110 & \text{Severe rockburst}\end{cases} \tag{13}$$

201 ### 3.3 Analysis and evaluation of rockburst proneness criterion

202 In order to further verify the rationality and superiority of the rockburst proneness criterion
203 proposed in this paper, taking rockburst disaster of typical engineering as examples (**Table 3**), E.
204 Hoek criterion, Russenes criterion, Erlangshan highway tunnel criterion, Gu-Tao criterion and the
205 rockburst proneness criterion proposed in this paper were tested respectively. The results were
206 compared with the actual rockburst intensity grade, as shown in **Table 4** and **Fig. 3**.

207 (1) E. Hoek criterion

208
$$\sigma_{\max}/\sigma_{\mathrm{c}}=\begin{cases}0.34 & \text{None rockburst}\\ 0.42 & \text{Weak rockburst}\\ 0.56 & \text{Moderate rockburst}\\ >0.70 & \text{Severe rockburst}\end{cases} \tag{14}$$

209 (2) Russenes criterion

210
$$\begin{cases}\sigma_\theta/\sigma_{\mathrm{c}}<0.2 & \text{None rockburst}\\ \sigma_\theta/\sigma_{\mathrm{c}}=0.2-0.3 & \text{Weak rockburst}\\ \sigma_\theta/\sigma_{\mathrm{c}}=0.3-0.55 & \text{Moderate rockburst}\\ \sigma_\theta/\sigma_{\mathrm{c}}>0.55 & \text{Severe rockburst}\end{cases} \tag{15}$$

211 (3) Erlangshan highway tunnel criterion

212
$$\begin{cases}\sigma_\theta/\sigma_{\mathrm{c}}<0.3 & \text{None rockburst}\\ \sigma_\theta/\sigma_{\mathrm{c}}=0.3-0.5 & \text{Weak rockburst}\\ \sigma_\theta/\sigma_{\mathrm{c}}=0.5-0.7 & \text{Moderate rockburst}\\ \sigma_\theta/\sigma_{\mathrm{c}}>0.7 & \text{Severe rockburst}\end{cases} \tag{16}$$

213 (4) Gu-Tao criterion

214
$$\begin{cases}\sigma_{\mathrm{c}}/\sigma_1>14.5 & \text{None rockburst}\\ \sigma_{\mathrm{c}}/\sigma_1=5.5-14.5 & \text{Weak rockburst}\\ \sigma_{\mathrm{c}}/\sigma_1=2.5-5.5 & \text{Moderate rockburst}\\ \sigma_{\mathrm{c}}/\sigma_1<2.5 & \text{Severe rockburst}\end{cases} \tag{17}$$

215 **Table 3** Initial data of rockburst disaster of typical engineering

216 **Table 4** Different criteria test results

217 **Fig. 3** Comparison of rockburst times based on different criteria

218 It can be seen from **Table 4** and **Fig. 3**: (1) the total number of moderate and severe rockbursts
219 determined by E. Hoek criterion, Russenes criterion and Erlangshan highway tunnel criterion is
220 relatively close, and the number of weak rockburst determined by E. Hoek criterion is slightly higher
221 than that determined by Russenes criterion and Erlangshan highway tunnel criterion; (2) the
222 rockburst grade determined by the Gu-Tao criterion is mainly concentrated in the moderate
223 rockburst, and the total number of weak and severe rockbursts is relatively close, which indicates
224 that the determination accuracy of Gu-Tao criterion is slightly lower than that of E. Hoek criterion,
225 Russenes criterion and Erlangshan highway tunnel criterion; (3) the total number of weak and
226 moderate rockbursts determined by the rockburst proneness criterion in this paper is close to the
227 actual situation, but its performance in the determination of severe rockburst grade is weak. By
228 comprehensive comparison, the accuracy of the criterion presented in this paper is obviously higher
229 than that of the other four criterions, and it is basically consistent with the actual occurrence of
230 rockburst on the whole, which has good engineering applicability.

231 In summary, the rockburst proneness criterion established in this study is of clear significance,
232 simple and practical, which can reasonably and quantitatively determine the occurrence and
233 intensity grade of rockburst geological disasters in the process of deep underground engineering
234 construction. It comprehensively considers the integrity factors, mechanical factors, brittle factors
235 and energy storage factors in the process of rockburst inoculation. This criterion is more targeted
236 for rockburst prediction and evaluation, and it has good engineering applicability.

4 Numerical simulation analysis

In this section, relying on the 2# diversion tunnel of Jinping II Hydropower Station, the feasibility of numerical simulation of rockburst process was verified by three-dimensional discrete element software (3DEC), and the accuracy and applicability of the rockburst proneness criterion proposed in this paper were tested. Then, numerical simulation analysis on the inoculation mechanism and evolution law of rockburst geological disasters in deep underground engineering under three-dimensional stress conditions was carried out to study the dynamic response law of surrounding rock of deep underground engineering under excavation disturbance.

4.1 Calculation model and boundary constraint conditions

The 2# diversion tunnel of Jinping II Hydropower Station was excavated from east to west. When the excavation reached the K11+027–K11+046 section, an severe rockburst occurred from the north wall to the spandrel (**Fig. 4**) (Zhou et al. 2015). The depth of rockburst pit is about 2 m. Through field investigation, it is not found that there is a control structural plane in this section, and the surrounding rock is fresh and complete, which is mainly T_{2b} marble. The section size of 2# diversion tunnel is shown in **Fig. 5**. According to the field monitoring results, the ground stress level of the tunnel section was high, which was shown in **Table 5**.

Fig. 4 Rockburst location of 2# headrace tunnel

Fig. 5 Section size of 2# headrace tunnel

Table 5 Ground stress grade of 2# headrace tunnel

According to the Saint-Venant principle and the influence range of tunnel excavation, the calculation model was established with 90 m transverse length, 80 m vertical height and 50 m longitudinal width. The numerical model is shown in **Fig. 6** and the arrangement of monitoring

points is shown in **Fig. 7**. In the dynamic calculation, in order to make the dynamic energy of the system absorb quickly and achieve convergence, Rayleigh damping was used, the minimum critical damping ratio was 0.05, and the minimum center frequency was 500 Hz. The upper boundary of the calculation model was the stress constraint boundary condition, and the vertical load of 51.46 MPa (field measurement) was applied. The lower boundary, front and rear boundary and left and right boundary of the calculation model were all displacement constraint boundary conditions. The peripheral boundary of the model was set as a static boundary, and dampers were set in the normal and tangential directions of the model to reduce or eliminate the elastic wave reflection generated by the simulation calculation, which provided the constraint effect equivalent to the infinite site for the calculation model.

Fig. 6 Numerical model

Fig. 7 Monitoring point arrangement of 2# headrace tunnel

4.2 Action form of blasting load

Since rockburst is a complex process generated instantaneously, detonating the pre-buried explosive in the cavern will instantly generate irresistible high temperature and high pressure gas, which expand rapidly in the interior of the cavern. The blast shock wave generated acts on the inner wall of the cavern and rapidly attenuates to stress wave. The whole process is very short and the duration is only a few milliseconds. Because the explosion mechanism and its influencing factors are extremely complex, it is difficult to quantitatively determine the details of the explosion process. In the numerical analysis, the blasting load is often assumed to be a triangular shock wave (Zhou et al. 2020), and the expression of the blasting load history curve of the triangular function is shown in **Eq.** (18). Through the secondary development of three-dimensional discrete element software,

281 the dynamic load is applied by using FISH programming language, which is applied to the tunnel
282 excavation profile by using APPLE command.

283
$$p(t)=\begin{cases}0 & t<0,\ t>t_{\mathrm{d}}\\ \dfrac{t}{t_{\mathrm{r}}}p_{\mathrm{m}} & 0\le t\le t_{\mathrm{r}}\\ \dfrac{t_{\mathrm{d}}-t}{t_{\mathrm{d}}-t_{\mathrm{r}}}p_{\mathrm{m}} & t_{\mathrm{r}}\le t\le t_{\mathrm{d}}\end{cases} \tag{18}$$

284 Where $p(t)$ is the blasting load pressure value at any moment; p_{m} is the peak blasting load, p_{m}=60
285 MPa; t_{r} is the time when the blasting load rises to the peak, t_{r}=0.3 ms; t_{d} is the time for the positive
286 pressure of the blasting load , t_{d}=1 ms.

287 **4.3 Constitutive relation and yield criterion**

288 In the numerical simulation, the selection of the constitutive model needs to have a high degree
289 of conformity with the mechanical properties of engineering materials. The Mohr-Coulomb yield
290 criterion, which describes the mechanical behavior of hard rock, is adopted for the constitutive
291 relation of the model to truly reflect the stress condition of surrounding rock (Peng 2008). The
292 failure envelope of the criterion corresponds to the shear yield function and the tensile stress yield
293 function, which is a flow rule related to the tensile failure.

294 The physical and mechanical parameters of surrounding rock refer to the inversion results of
295 ground stress and mechanical parameters of rock mass of Jinping Project Group, Institute of Rock
296 and Soil Mechanics, Chinese Academy of Sciences, as shown in **Table 6**, where c_{m} is the peak value
297 of cohesion, c_{r} is the residual value of cohesion, φ_0 is the initial value of friction angle, φ_{m} is the
298 peak value of friction angle, and ψ is the dilatancy angle. The rock lithology is assumed in the
299 numerical calculation: the rock is homogeneous, isotropic continuum, which conforms to Mohr
300 Coulomb strength criterion, and the material parameters meet Mohr Coulomb constitutive model.

301 **Table 6** Physical and mechanical parameters of surrounding rock

302 4.4 Analysis of numerical simulation results

303 The middle position of the rockburst area (near K11+037) was selected for analysis. In the
304 numerical simulation, the FISH programming language embedded in 3DEC software was used to
305 write calculation functions for **Eq.** (2), **Eq.** (7) and **Eq.** (12), and the change process of all
306 calculation block units was monitored. In this section, the rockburst proneness would be evaluated
307 according to the numerical simulation results and the prediction evaluation indexes.

308 4.4.1 Analysis of energy release evolution process

309 According to the numerical simulation results, the distribution state of elastic strain energy
310 density was shown in **Fig. 8**, the contour nephogram of principal stress difference was shown in **Fig.**
311 **9**, and the space-time distribution of elastic strain energy density was shown in **Fig. 10**. From the
312 above figure, it could be seen that the maximum principal stress difference was mostly concentrated
313 in the right spandrel, side wall and arch bottom of the cavern after excavation. According to the rock
314 mechanics theory, the energy storage limit of rock mass at the maximum principal stress difference
315 will increase significantly. Combined with the cloud map of the elastic strain energy density
316 distribution, it was found that the surrounding rock masses close to the empty surface of the cavern
317 under the disturbance of dynamic excavation had different degrees of elastic strain energy release
318 phenomenon, and the amount of elastic strain energy release gradually decreased with the increase
319 of the distance to the center of the tunnel. The elastic strain energy release of surrounding rock at
320 the right spandrel, side wall and arch bottom of the cavern was the largest, which further indicated
321 that the gentle acceleration process of rock fracture evolution around the cavern is also the process
322 of energy accumulation and dissipation in the surrounding rock. The stress of surrounding rock was

highly concentrated, which increased the energy accumulation. When the storage energy of surrounding rock exceeded the energy storage limit of rock mass, the excess energy was released rapidly in the form of kinetic energy, resulting in rockburst or large deformation failure of rock mass.

The rockburst simulation was shown in **Fig. 11**. It could be seen from **Fig. 11** that the largest rockburst pit of the tunnel was located at the right side wall and spandrel of the tunnel face, which was close to the field situation, and the depth of the largest rockburst pit was about 2 m, as shown in **Fig. 12**. According to the failure shape of the tunnel, the numerical simulation results were basically consistent with the shape of the actual rockburst pit (**Fig. 13**), which verified the rationality of the prediction and evaluation of the rockburst criterion in this paper, and could meet the requirements of dynamic tracking of the rockburst process.

Fig. 8 Distribution of elastic strain energy density (unit: J/m^3)

Fig. 9 Contour nephogram of principal stress difference (unit: Pa)

Fig. 10 Space-time distribution of elastic strain energy density

Fig. 11 Rockburst simulation

Fig. 12 Rockburst areas in situ

Fig. 13 Tunnel section outline

4.4.2 Distribution characteristics of rock burst energy index

The nephogram of the boundary value distribution of rockburst proneness criterion was shown in **Fig. 14**. From **Fig. 14**, it could be seen that the rockburst criterion RPC boundary value at different locations of the tunnel section showed a completely different change rule. Details were as follows: at the right spandrel position of the cavern, the RPC boundary value reached the maximum 121.23; at the junction of the spandrel and the side wall on both sides of the cave, the RPC boundary values

were mostly concentrated between 40 and 85, which could release some elastic strain energy and had the possibility of moderate rockburst; at the left spandrel of the cavern, the RPC boundary values were mostly concentrated between 95 and 120, and there was a possibility of severe rockburst. This shows that the surrounding rock accumulates a large number of elastic strain energy under the influence of high stress. When the surrounding rock strength exceeds the ultimate strength of the rock mass, the surrounding rock occurs brittle failure and instantaneous releases a large number of elastic strain energy, and then the rockburst phenomenon of rock block spalling, ejection and even throwing occurs.

Taking the arch foot on the right side of the cavern as the center of the circle and rotating counterclockwise for one round, the RPC boundary value of the cavern cross section (0°–360°) of the section K11+037 was obtained, as shown in **Fig. 15**. According to the analysis of **Fig. 15**, the maximum value of RPC boundary value appeared on the surrounding rock surface of the cavern spandrel (about 70°–85°). When the angle was 0°–90°, the boundary value of RPC was 12–96, and there was a possibility of weak to severe rockburst. When the angle was 90°–180°, the boundary value of RPC was 30–95, and there was a possibility of moderate to severe rockburst. When the angle was 180°–240°, the boundary value of RPC was 25–70, and there was a possibility of moderate rockburst. When the angle was 240°–360°, the boundary value of RPC was 45–90, and there was a possibility of moderate to severe rockburst. From the above analysis, it could be seen that the RPC boundary value obtained by numerical simulation was consistent with the case of severe rockburst in practical engineering.

Fig. 14 Nephogram of the boundary value distribution of RPC

Fig. 15 RPC thresholds of the cavern cross section (0°–360°) of the section K11+037

5 Conclusion

(1) Based on the energy principle and taking the rock strength and overall failure criterion as the benchmark, we established the rockburst proneness criterion of rock mass unit under compression and tension and proposed three rockburst classification thresholds for four grades of none, weak, moderate and severe rockburst.

(2) Taking the typical rockburst disaster as examples, the rationality of the existing classical rockburst criterions and the rockburst proneness criterion proposed in this paper were tested, and the results showed that this criterion was simple and practical and had good engineering applicability, which took into account the integrity factors, mechanical factors, brittleness factors and energy storage factors in the process of rockburst inoculation.

(3) Numerical simulation analysis of rockburst disaster in $2^{\#}$ diversion tunnel of Jinping II hydropower station was carried out by using this criterion. The results were basically consistent with the actual situation, which verified the accuracy and effectiveness of the rockburst proneness criterion proposed in this paper.

Acknowledgments

This study was financially supported by the National Natural Science Foundation of China (Grant No.: 51474097, U1810203).

Disclosure statement

The authors declare that they have no conflicts of interest.

References

Barton N, Lien R, Lunde J (1974) Engineering classification of rock masses for the design of tunnel support. Rock Mechanics 6(4): 189-236.

BIENIAWSKI ZT (1967) Mechanism of brittle fracture of rock. International Journal of Rock Mechanics and Mining Sciences & Geomechanics Abstracts 4(4): 405-430.

Chen BR, Feng XT, Xiao YX, Ming HJ, Zhang CS, Hou J, Chu WJ (2010) Acoustic Emission Test on Damage Evolution of Surrounding Rock in Deepburied Tunnel during TBM Excavation. Chinese Journal of Rock Mechanics and Engineering 29(8): 1562-1569.

Cook NG (1965) A note on rockbursts considered as a problem of stability. South African Institute of Mining and Metallugy 5(65): 437-446.

Feng XT, Chen BR, Zhang CQ, Li SJ, Wu SY (2013) Mechanism, warning and dynamic control of rockburst development processes. Beijing: Science Press.

Feng XT, Xiao YX, Feng GL, Yao ZB, Chen BR, Yang CX, Su GS (2019) Study on the development process of rockbursts. Chinese Journal of Rock Mechanics and Engineering 38(4): 649-673.

Feng XT, Zhang CQ, Chen BR, Feng GL, Zhao ZN, Ming HJ, Xiao YX, Duan SQ, Zhou H (2012) Dynamical control of rockburst evolution process. Chinese Journal of Rock Mechanics and Engineering 31(10): 1983-1997.

Gong FQ, Wang YL, Luo S (2020) Rockburst proneness criteria for rock materials: Review and new insights. Journal of Central South University 27(10): 2793-2821.

Gu MC, He FL, Chen CZ (2002) Study on rockburst in Qinling tunnel. Chinese Journal of Rock Mechanics and Engineering 21(9): 1324-1329.

Guo JQ, Zhao Q, Wang JB, Zhang J (2015) Rockburst prediction based on elastic strain energy.

411 Chinese Journal of Rock Mechanics and Engineering 34(9): 1886-1893.
412 Hoek EP, Brown ET (1997) Practical estimates of rock mass strength. International Journal of Rock
413 Mechanics and Mining Sciences 34(8): 1165-1186.
414 John CJ, Neville GW (1979) Fundamentals of rock mechanics. Science Paperbacks 9(3): 251-252.
415 Karchevsky AL (2017) Determination of the possibility of rock burst in a coal seam. Journal of
416 Applied and Industrial Mathematics 11(4): 527-534.
417 Kidybinnski A (1981) Bursting liability indices of coal. International Journal of Rock Mechanics
418 and Mining Sciences & Geomechanics Abstracts 18(2): 295-304.
419 Li XB, Gong FQ, Wang SF, Li DY, Tao M, Zhou J, Huang LQ, Ma CD, Du K, Feng F (2019)
420 Coupled static-dynamic loading mechanical mechanism and dynamic criterion of rockburst in
421 deep hard rock mines. Chinese Journal of Rock Mechanics and Engineering 38(4): 708-723.
422 Li ZY, Wu G, Huang TZ, Liu Y (2018) Variation of energy and criteria for strength failure of shale
423 under traixial cyclic loading. Chinese Journal of Rock Mechanics and Engineering 37(3): 662-
424 670.
425 Ma TH, Tang CA, Tang LX, Zhang WD, Wang L (2015) Rockburst characteristics and microseismic
426 monitoring of deep-buried tunnels for Jinping II Hydropower Station. Tunnelling and
427 Underground Space Technology 49: 345-368.
428 Ministry of Water Resources of the People's Republic of China. (2014) GB/T50218-2014 Standard
429 for engineering classification of rock mass. Beijing: China Planning Press.
430 Mitri H (1999) FE modelling of mining-induced energy release and storage rates. Journal South
431 African Institute of Mining and Metallurgy 99(2): 103-110.
432 Peng WB (2008) Practical of FLAC3D. Beijing: China Machine Press.

433 Qiu SL, Feng XT, Jiang Q , Zhang CQ (2014) A novel numerical index for estimating strainburst
434 vulnerability in deep tunnels. Chinese Journal of Rock Mechanics and Engineering 33(10):
435 2007-2017.
436 Roohollah SF, Abbas T (2018) Long-term prediction of rockburst hazard in deep underground
437 openings using three robust data mining techniques. Engineering with Computers 35(9): 659-
438 675.
439 Russnes BF (1974) Analyses of rockburst in tunnels in valley sides. Trondheim: Norwegian Institute
440 of Technology.
441 Ryder JA (1988) Excess shear stress in the assessment of geologically hazardous situations. Journal
442 South African Institute of Mining and Metallurgy 88(1): 27-39.
443 Shang YJ, Zhang JJ, Fu BJ (2013) Analyses of three parameters for strain mode rockburst and
444 expression of rockburst potential. Chinese Journal of Rock Mechanics and Engineering 32(8):
445 1520-1527.
446 Su GS (2006) Study on stability analysis and intelligent optimization for large underground caverns
447 under high geostress condition. Wuhan: Graduate University of Chinese Academy of Sciences.
448 Wang YH, Li WD, Li QG, Xu Y, Tang GH (1998) Method of fuzzy comprehensive evaluations for
449 rockburst prediction. Chinese Journal of Rock Mechanics and Engineering 17(5): 493-501.
450 Wei XJ, Chen TT, Wang X, Yu XF, Zhou LY (2020) Progress in research of the rockburst hazard.
451 Modern Tunnelling Technology 57(2): 1-12.
452 WILES TD (1998) Correlation between local energy release density observed bursting conditions
453 at Creighton Mine. Sudbury, Canada: Mines Research.
454 Wu QB (1993) Application of microgravity method in rockburst prediction. Progress in Geophysics

455 8(3): 136-142.
456 Xie HP, Ju Y, Li LY (2005) Criteria for strength and structural failure of rocks baded on energy
457 dissipation release principles. Chinese Journal of Rock Mechanics and Engineering 24(17):
458 3003-3010.
459 Xu B, Xie HP, Tu YJ (2007) Numerical simulation of rockburst stress state during excavation of
460 underground powerhouse of Pubugou Hydropower Station. Chinese Journal of Rock
461 Mechanics and Engineering 26(S1): 2894-2900.
462 Xu LS, Wang LS (1999) Study on the laws of rockburst and its forecasting in the tunnel of Erlang
463 Mountain road. Chinese Journal of Geotechnical Engineering 21(5): 569-572.
464 Zhang CQ, Feng XT, Zhou H, Qiu SL, Wu WP (2012) Case histories of four extremely intense
465 rockbursts in deep tunnels. Rock Mechanics and Rock Engineering 45 (3): 275-288.
466 Zhang CQ, LU JJ, Chen J, Zhou H, Yang FJ (2017) Discussion on rockburst proneness indexes and
467 their relation. Rock and Soil Mechanics 38(5): 1397-1404.
468 Zhang JJ, Fu BJ (2008) Rockburst and its criteria and control. Chinese Journal of Rock Mechanics
469 and Engineering 27(10): 2034-2042.
470 Zhang JJ, Fu BJ, Li ZK, Song SW, Shang YJ (2011) Criterion and classification for strain mode
471 rockbursts based on five-factor comprehensive method//Qian Q H, Zhou Y X, ed.
472 Harmnonising Rock Engineering and the Environment.562-563.
473 Zhang SC, Ma TH, Tang CA, Jia P, Wang YC (2020) Microseismic monitoring and experimental
474 study on mechanism of delayed rockburst in deep-buried tunnels. Rock Mechanics and Rock
475 Engineering 53(6): 2771-2788.
476 Zhang YB, Yang Z, Yao XL (2018) Experimental study on real-time early warning method of tunnel

rock burst based on infrared radiation spatial and temporal evolutions. Journal of Mining and Safety Engineering 35(2): 299-307.

Zhou H, Chen SK, Zhang GZ, Wang HL, He HD, Feng J (2020) Rockburs predicition in deep lying and long tunnel based on efficiency coefficient method and ground stress filed inversion. Journal of Engineering Geology 34(2): 1-11.

Zhou H, Yang FJ, Zhang CQ, Lu JJ (2015) Methods for numerical simulation and evaluation of rock burst and rock burst. Beijing: Science Press.

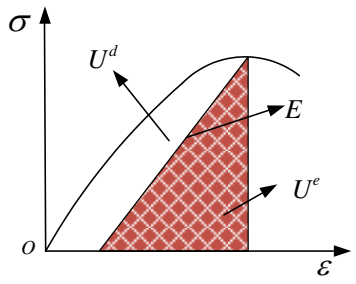

485

486 **Fig. 1** Stress-strain relation curve of rock

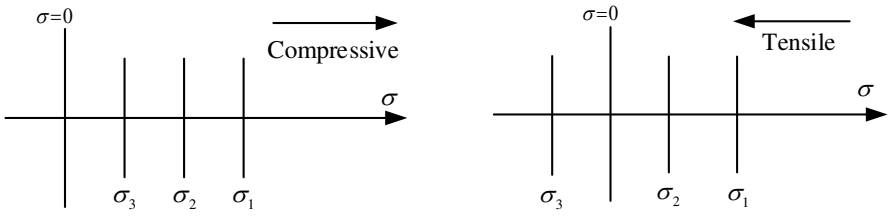

(a) Compression condition (b) Tension condition

Fig. 2 Loading condition

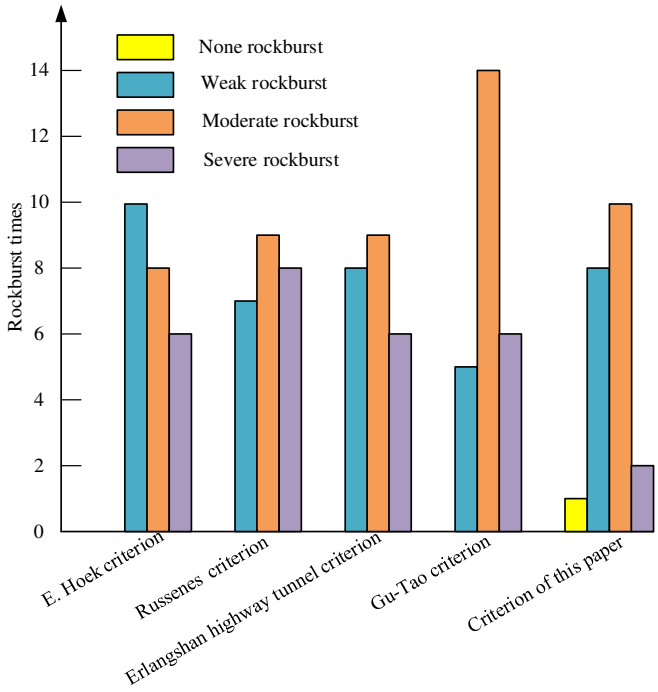

489

490

Fig. 3 Comparison of rockburst times based on different criteria

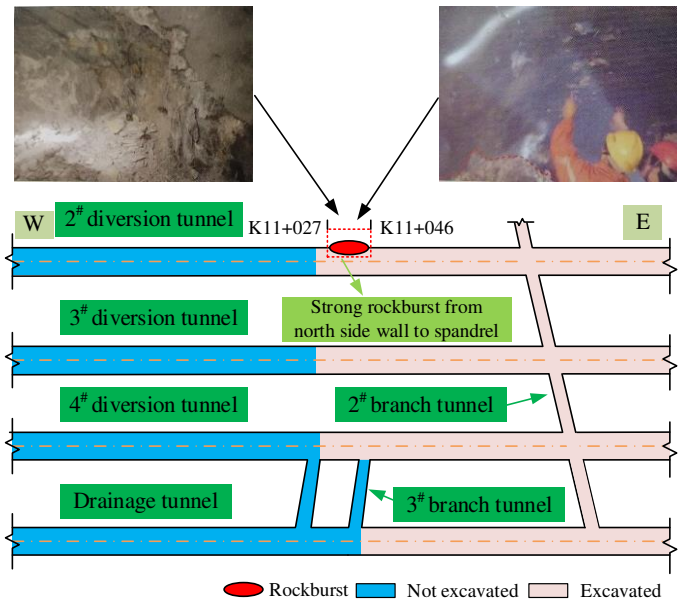

Fig. 4 Rockburst location of 2# headrace tunnel

493

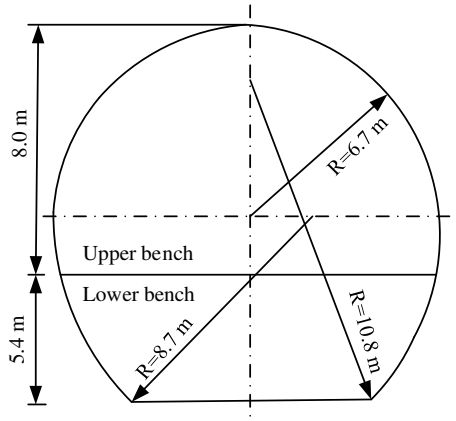

Fig. 5 Section size of 2# headrace tunnel

494

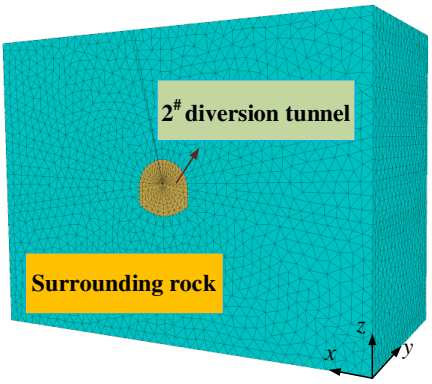

495

Fig. 6 Numerical model

496

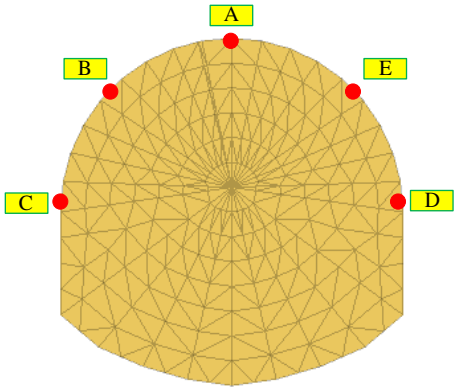

497

Fig. 7 Monitoring point arrangement of 2# headrace tunnel

498

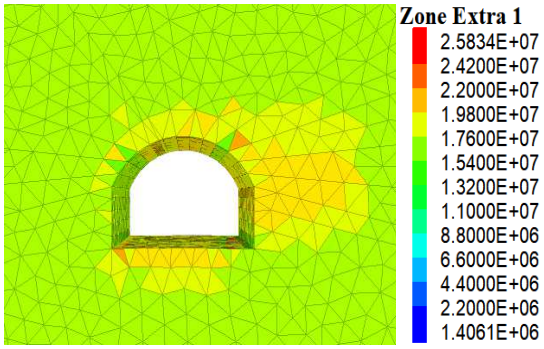

499

Fig. 8 Distribution of elastic strain energy density (unit: J/m^3)

500

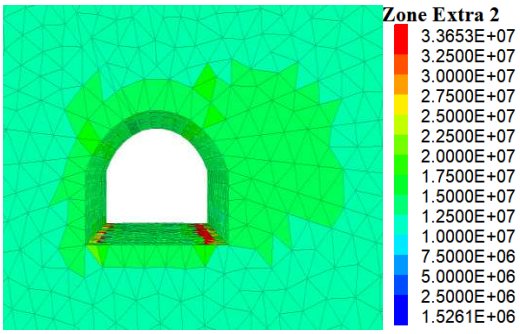

501

502 **Fig. 9** Contour nephogram of principal stress difference (unit: Pa)

503

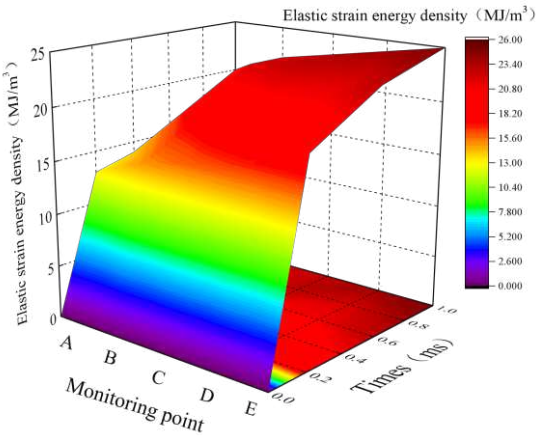

Fig. 10 Space-time distribution of elastic strain energy density

504

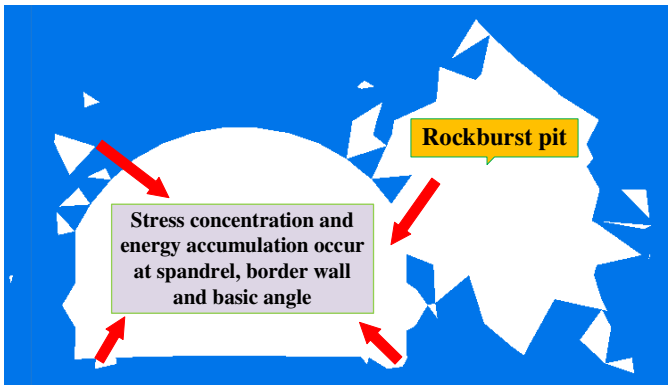

505

Fig. 11 Rockburst simulation

506

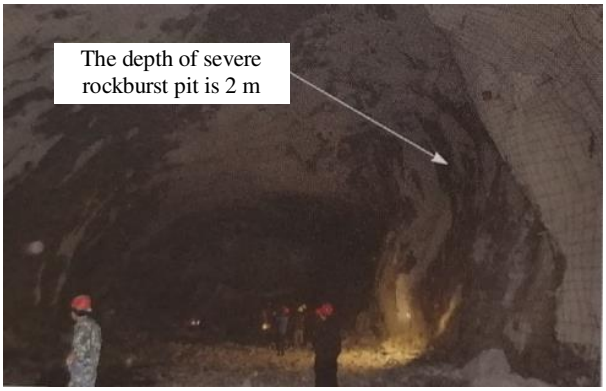

507

Fig. 12 Rockburst areas in situ

508

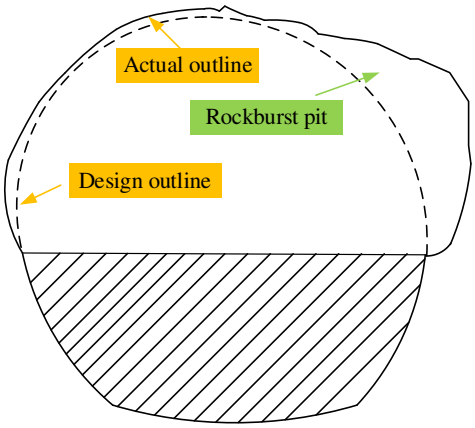

509

Fig. 13 Tunnel section outline

510

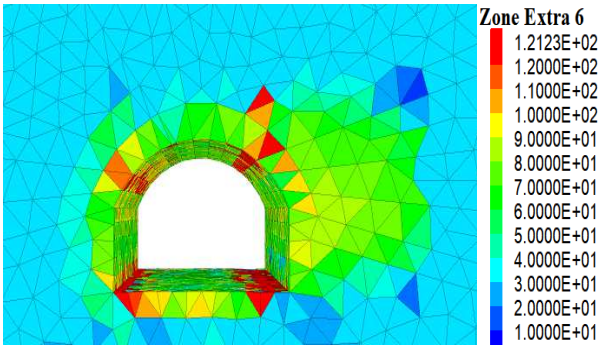

511

Fig. 14 Nephogram of the boundary value distribution of RPC

512

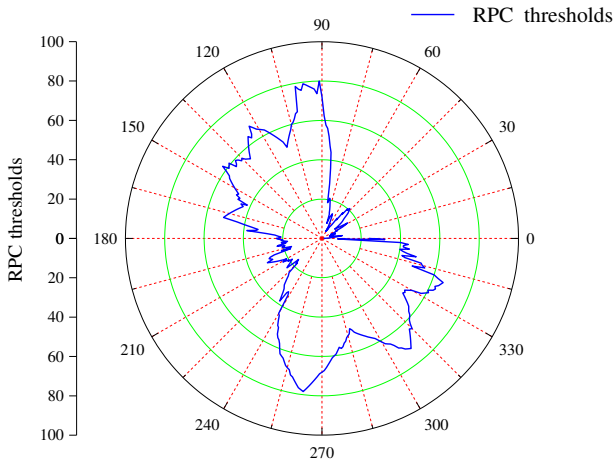

513

Fig. 15 RPC thresholds of the cavern cross section (0°–360°) of the section K11+037

514

515 **Table 1** Measured data of rockburst of Tiantaishan tunnel

No.	Position/m	Level of rockburst	Evaluation results of different evaluation methods					
			K_u	Rockburst proneness	σ_c/σ_{max}	Rockburst proneness	R	Rockburst proneness
TSE5	108	Weak	3.1	Weak	8.1	Weak	0.8	None
	150	Moderate	2.7	Weak	7.3	Weak	2.7	Weak
	271–350	Weak	2.7	Weak	8.4	Weak	1.5	None
TSE6	500–550	Moderate	2.8	Weak	4.7	Weak	7.6	Weak
	350	Weak	–	–	7.4	Weak	1.4	None
	500	Moderate	–	–	5.1	Moderate	11.6	Moderate

516

517 **Table 2** Simulation results of rockburst of Tiantaishan tunnel

518

No.	Position/m	σ_i /MPa			v	K_v	σ_c/MPa	σ_t/MPa
		σ_1	σ_2	σ_3				
TSE5	108	16.15	8.14	4.27	0.28	0.68	130.21	11.55
	150	19.23	10.51	3.16			141.13	13.68
	271–350	20.22	12.53	3.58			169.52	15.14
TSE6	500–550	40.57	24.12	12.36	0.28	0.68	192.15	18.86
	350	23.65	10.87	4.02			175.65	17.26
	500	35.86	21.44	15.61			184.27	18.34

Annotation: K_u is the deformation brittleness coefficient; σ_{max} is maximum principal stress of surrounding rock; σ_c/σ_{max} is surrounding rock strength ratio.

519

Table 3 Initial data of rockburst disaster of typical engineering

520

521

No.	Engineering	Buried depth/m	σ /MPa			σ_{max} /MPa	σ_c /MPa	K_v
			σ_1	σ_2	σ_3			
1	Jinping I hydropower station	400	9.00	8.44	4.50	18–70	50–70	0.34–0.72
			35.00	17.50	10.80			
2	Jinping II hydropower station	1200–2500	38.00	32.40	19.00	55–108	110–120	0.76
			71.00	67.50	35.50			
3	Diversion tunnel for TianshengqiaoII hydropower station	130–760	25.80	12.90	3.51	30	88.7	0.75
			25.80	20.52	12.90			
4	Diversion tunnel for Taipingyi hydropower station	400	31.40	15.70	10.80	62.6	130–180	0.75
5	Qinling railway Tunnel	1600	20.00	18.75	10.00	105	95–130	0.75
			40.00	37.50	20.00			
6	Shandong Linglong gold mine	1000	50.00	27.00	25.00	82–114	138–197	0.75
			60.00	30.00	27.00			
7	Erlangshan highway tunnel	770	53.70	26.85	20.79	41.46	64.9	0.75
8	Tongling Dongguashan copper mine	790–850	34.33	21.33	17.17	105.5	132.2	0.75
			34.33	22.95	17.17			
			57.20	28.60	10.80			
9	Underground caverns of Pubugou hydropower station	250–320	27.30	13.65	8.64	42–54	82.3–207.5	0.80
			21.10	10.55	6.75			
10	Diversion tunnel for Yuzixi I hydropower station	250–600	45.00	22.50	16.20	90	170	0.80
			30.00	15.00	6.75			
11	Tai-Jin expressway Cangling tunnel	300–756	59.50	29.75	8.10	48.9	150	0.75
			59.50	29.75	20.41			

522

Table 4 Different criteria test results

523

No.	σ_t/MPa	E.Hoek criterion		Russenes criterion	Erlangshan highway tunnel criterion	Gu-Tao criterion		The criterion of this paper	
		Threshold	Grade of ockburst	Grade of rockburst	Grade of rockburst	Threshold	Grade of rockburst	Threshold	Grade of rockburst
1	5.0	0.36	Weak	Moderate	Weak	5.56	Weak	0.4	None
		1.40	Severe	Severe	Severe	1.43	Severe	10.6	Weak
2	5.0–6.0	0.50	Moderate	Moderate	Moderate	2.89	Moderate	137.9	Severe
		0.46	Weak	Moderate	Weak	1.55	Severe	569.9	Severe
3	3.7	0.34	Weak	Weak	Weak	3.44	Severe	23.8	Moderate
		0.34	Weak	Weak	Weak	3.44	Severe	98.8	Moderate
4	9.4	0.35–0.48	Weak-Moderate	Weak-Moderate	Weak	4.14–5.73	Moderate-Severe	6.2	Weak
5	7.0	1.11	Severe	Severe	Severe	4.75–6.50	Weak-Moderate	7.7	Weak
		0.81	Severe	Severe	Severe	2.38–3.25	Moderate	61.7	Moderate
6	7.0–10.0	0.59	Moderate	Severe	Moderate	2.76	Moderate	90.9	Moderate
		0.42	Weak	Moderate	Weak	3.94	Moderate	31.2	Moderate
7	8.0	0.64	Moderate	Severe	Moderate	1.21	Severe	56.6	Moderate
8	16.4	0.80	Severe	Severe	Severe	3.85	Moderate	2.4	Weak
9	5.9	0.20–0.51	Severe	Severe	Severe	3.01–7.60	Moderate	17.3	Weak
		0.26–0.66	Severe	Severe	Severe	3.90–9.83	Moderate	8.1	Weak
10	11.3	0.53	Weak-Moderate	Weak-Moderate	Weak-Moderate	3.78	Weak-Moderate	12.5	Moderate
		0.53	Weak-Moderate	Weak-Moderate	Weak-Moderate	5.67	Weak-Moderate	2.4	Weak
11	8.0	0.33	Moderate	Moderate	Moderate	2.52	Moderate	28.9	Moderate
		0.33	Moderate	Moderate	Moderate	2.52	Moderate	68.3	Weak

524 **Table 5** Ground stress grade of $2^{\#}$ headrace tunnel

525

Buried depth/m	σ_x / MPa	σ_y / MPa	σ_z / MPa	τ_{xy} / MPa	τ_{yz} / MPa	τ_{zx} / MPa
1900	-48.54	-49.97	-51.46	-0.35	-3.23	-5.82

Table 6 Physical and mechanical parameters of surrounding rock

E/GPa	v	c_m/MPa	c_r/MPa	φ_0/(°)	φ_m/(°)	ψ/(°)
18.9	0.23	15.6	7.4	25.8	39.0	10.0

Figures

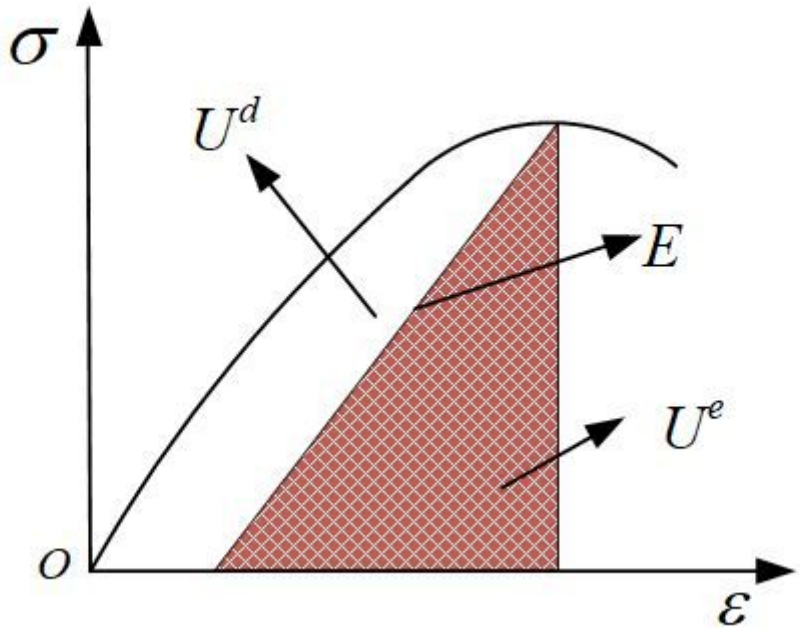

Figure 1

Stress-strain relation curve of rock

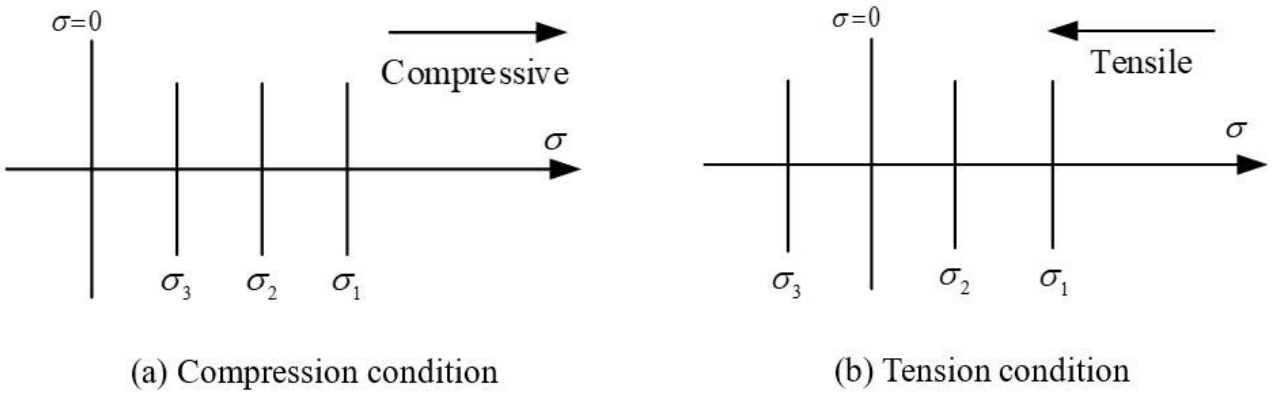

Figure 2

Loading condition

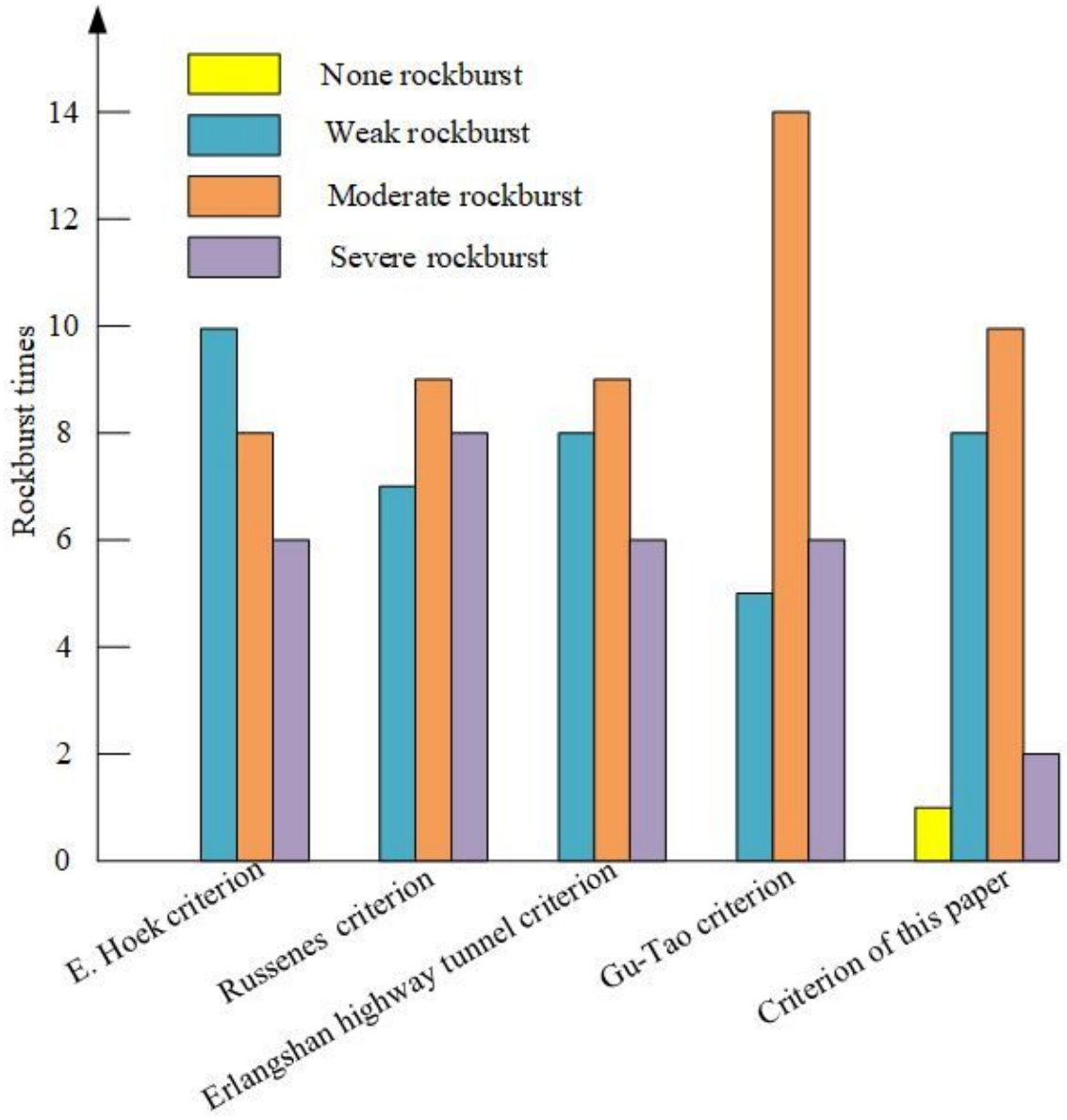

Figure 3

Comparison of rockburst times based on different criteria

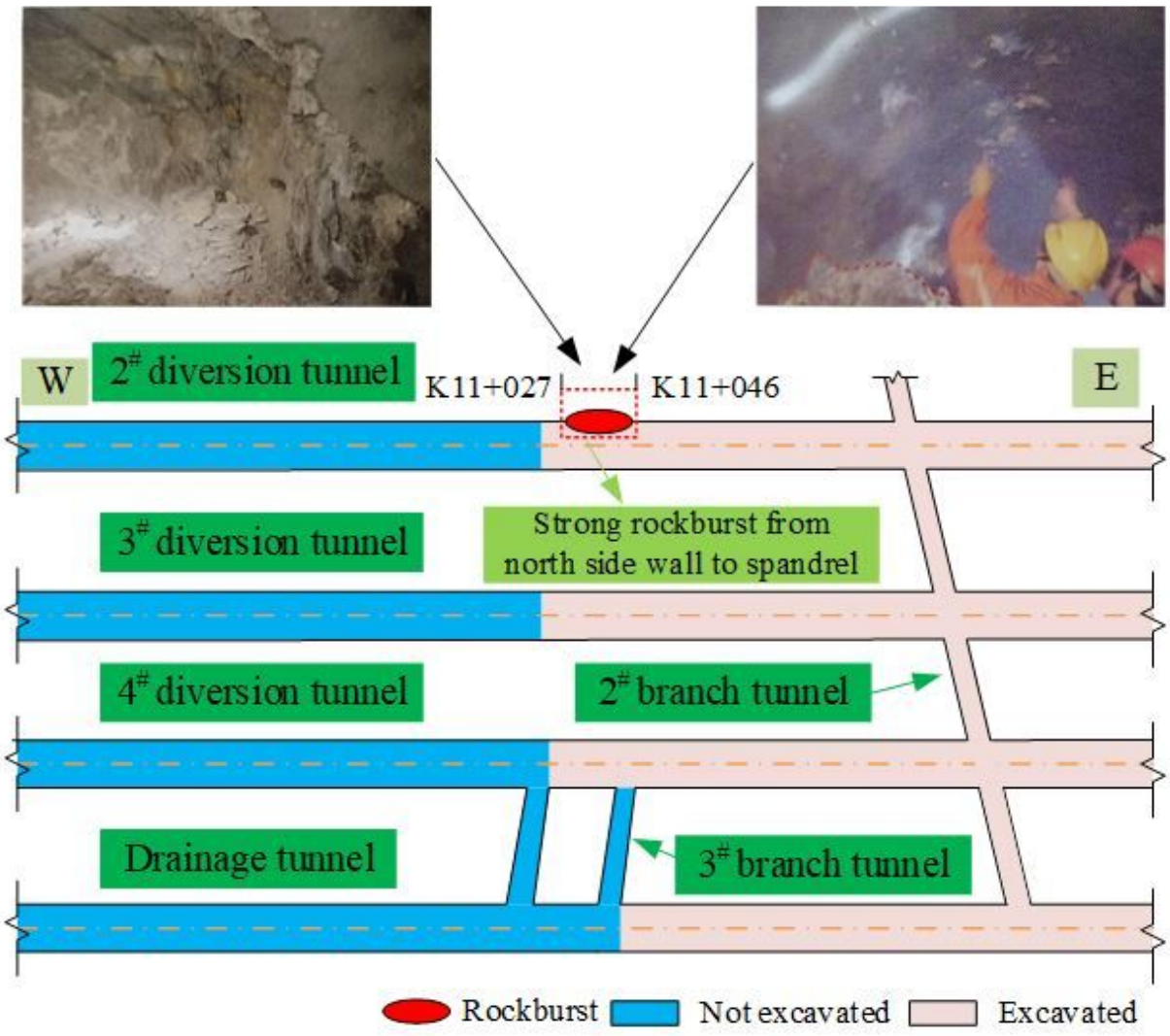

Figure 4

Rockburst location of 2# headrace tunnel

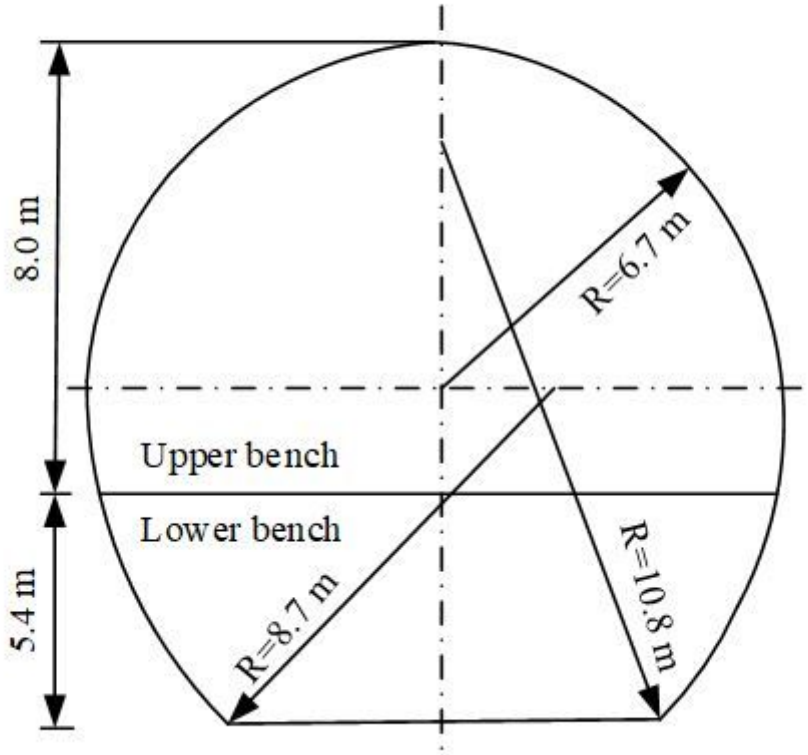

Figure 5

Section size of 2# headrace tunnel

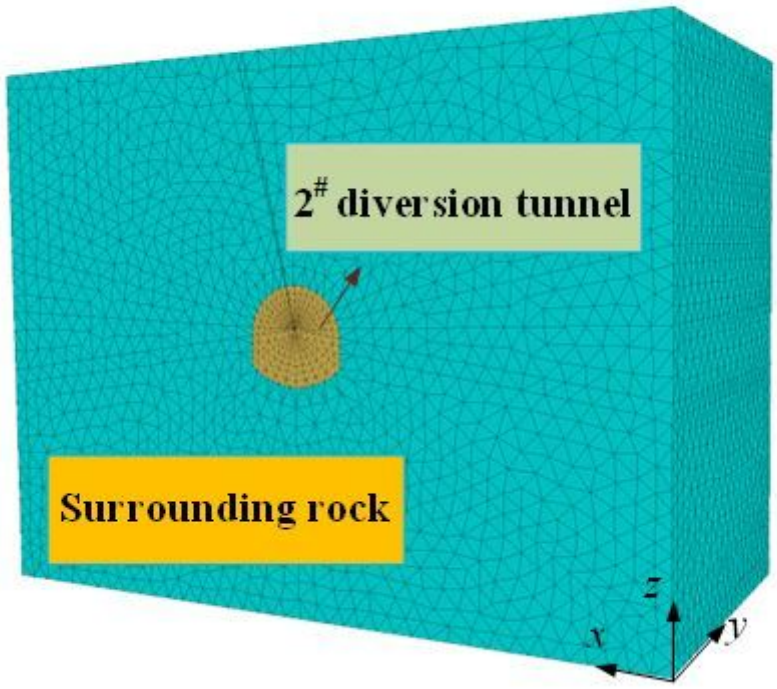

Figure 6

Numerical model

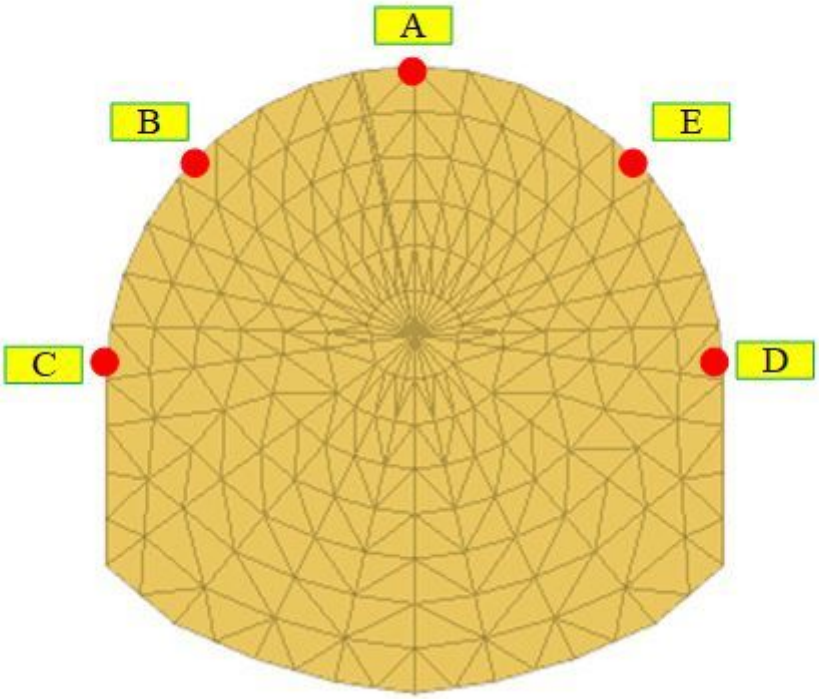

Figure 7

Monitoring point arrangement of 2# headrace tunnel

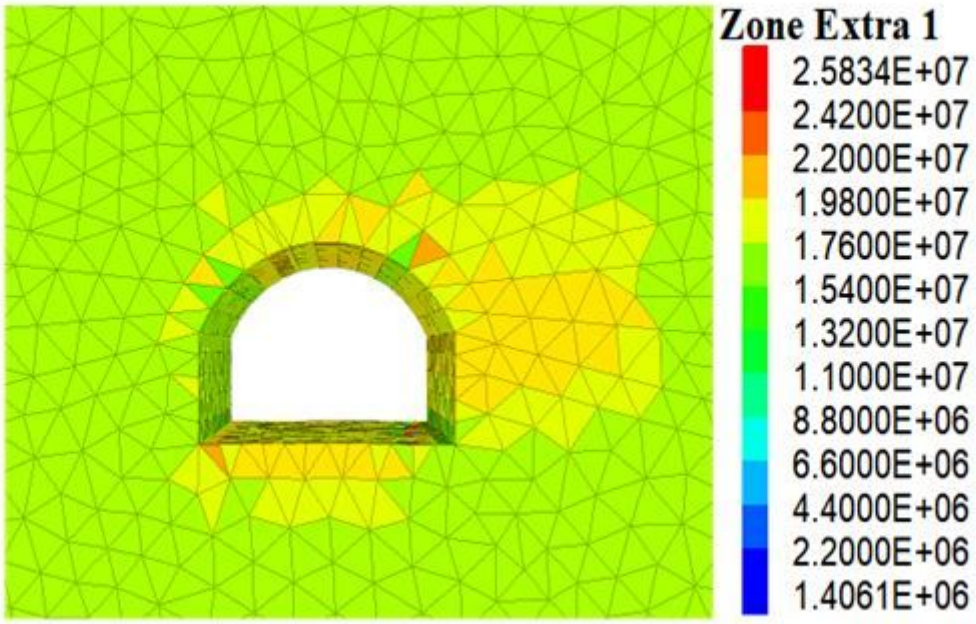

Figure 8

Distribution of elastic strain energy density (unit: J/m3)

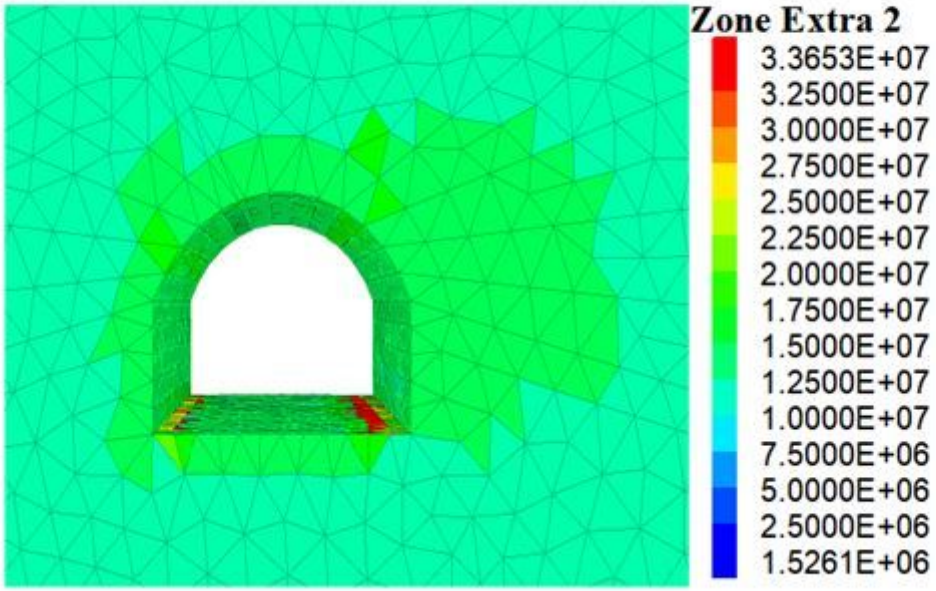

Figure 9

Contour nephogram of principal stress difference (unit: Pa)

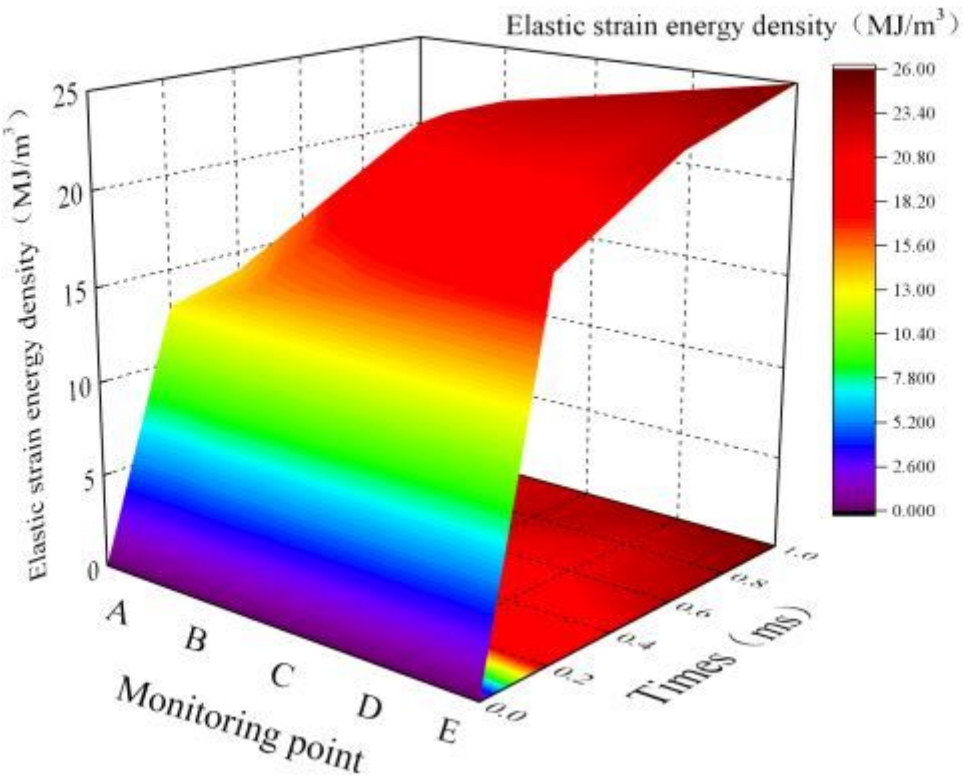

Figure 10

Space-time distribution of elastic strain energy density

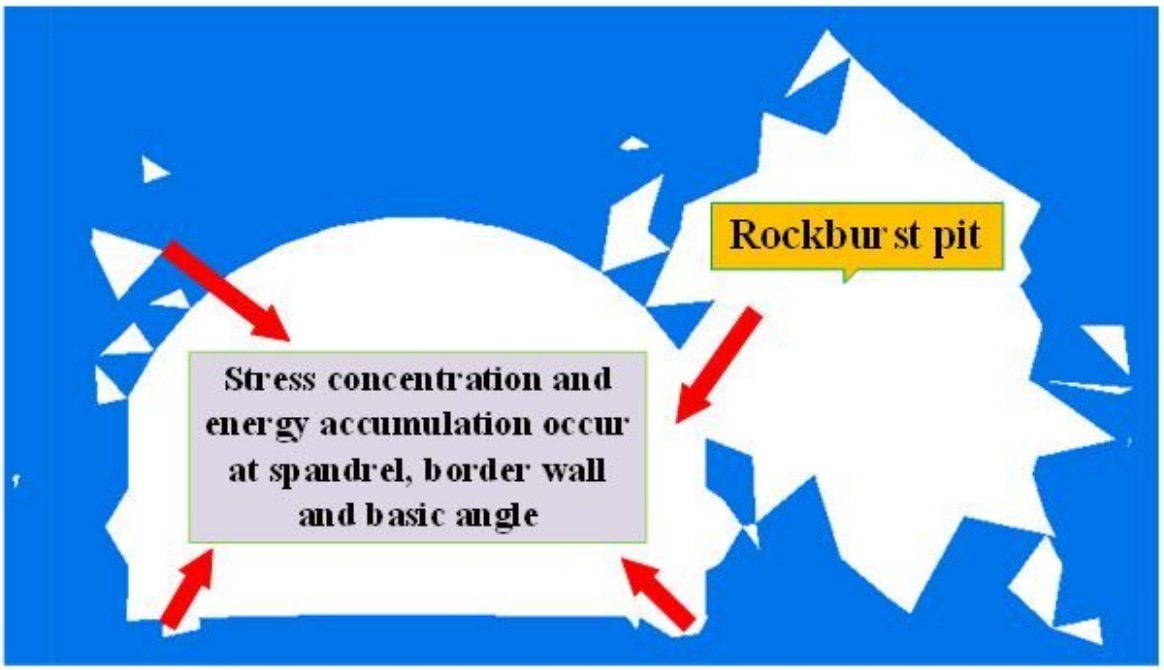

Figure 11

Rockburst simulation

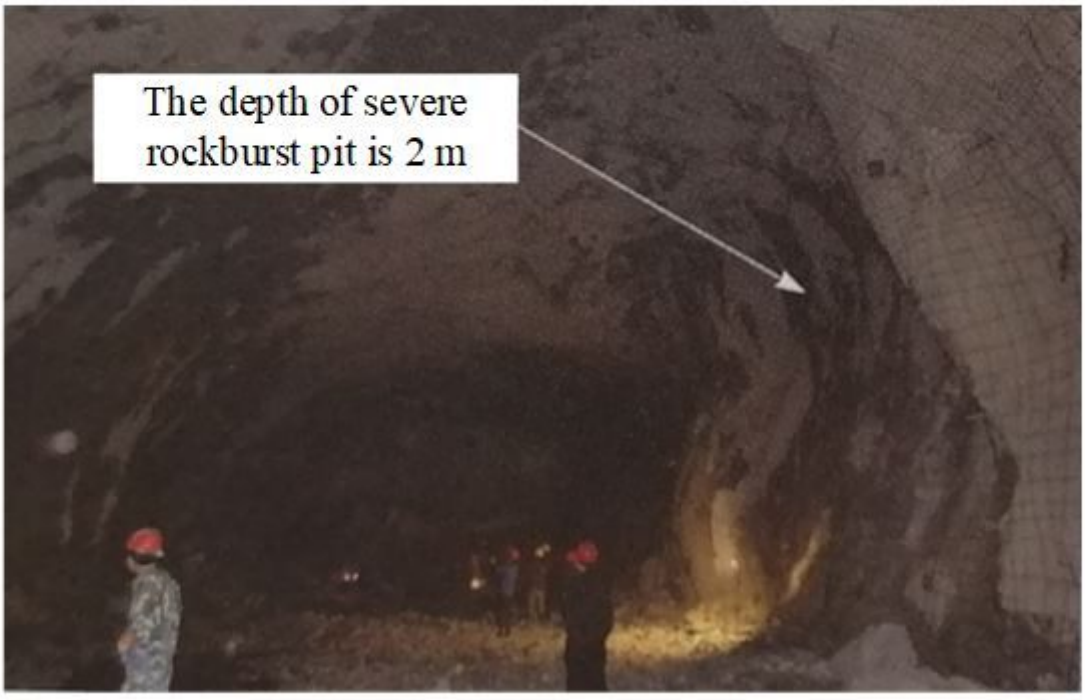

Figure 12

Rockburst areas in situ

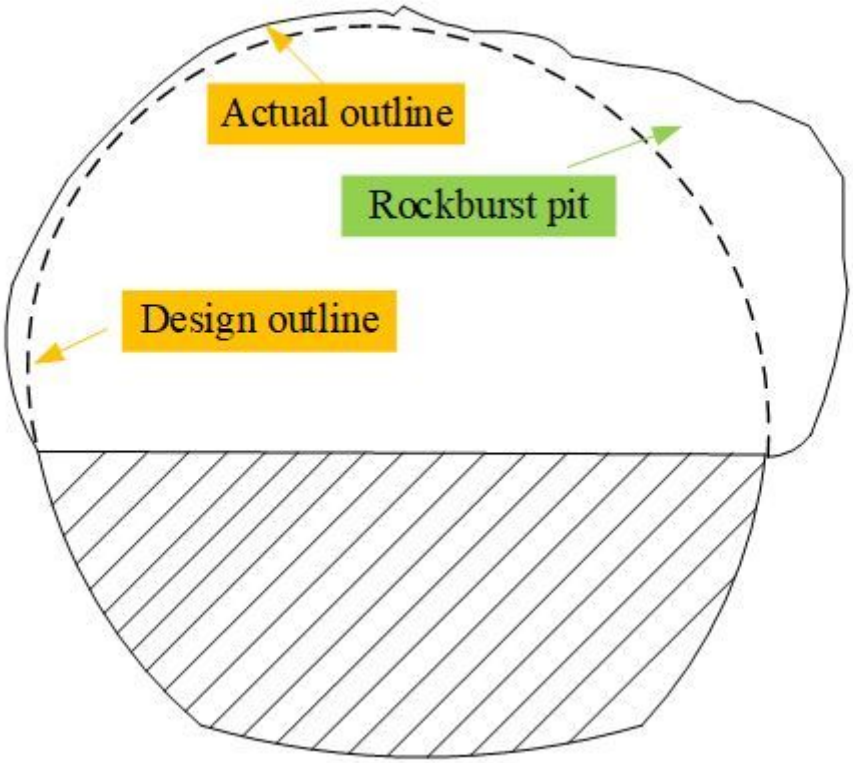

Figure 13

Tunnel section outline

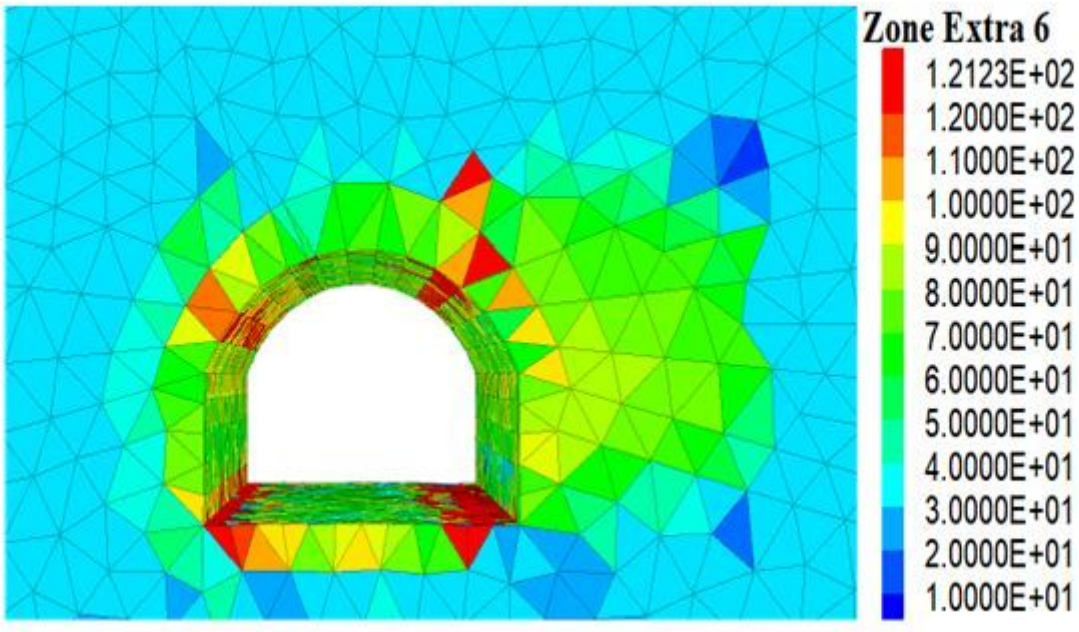

Figure 14

Nephogram of the boundary value distribution of RPC

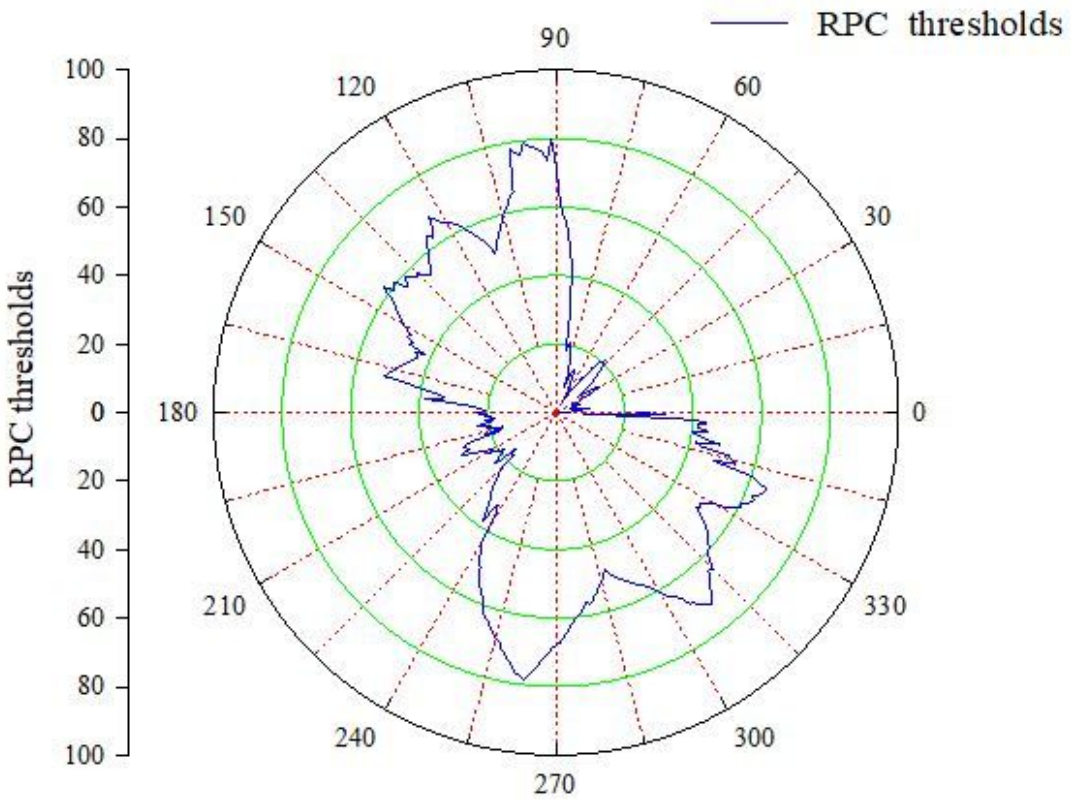

Figure 15

RPC thresholds of the cavern cross section (0°–360°) of the section K11+037